CHAPTER-5

Synthesis, Characterization, and Study of High-k Dielectricity of Bulk Pristine Fe^{3+} and Li^{+} Co-substituted Wurtzite ZnO

5.1 Introduction

ZnO is an n-type semiconductor with a large band gap of 3.37 eV at room temperature, high excitation binding energy of 60 meV, high transparency, and biocompatibility & thermally stability [1]. Due to these properties, ZnO draws much attention and it can be used in a large variety of applications like preparing high-temperature stable high-permittivity electric material, solar cells[2], light-emitting devices[3], gas sensors[4,5], piezoelectric devices[6], photo-catalysis[7], DNA sequence detectors[8], and field emission transistors[9]. High dielectric constant materials are of technological importance as they lead to the miniaturization of electronic devices. ZnO has attracted considerable attention because it can be used for a wide range of applications including dielectrics. Although the dielectric properties of ZnO nanostructures, films, and ceramics have been investigated by many researchers, further improvements are still required before they become viable for commercial applications in devices [10-12], and the material can be utilized in different applications due to its low cost [13-16], non-toxicity [17,18] and bio-compatibility [19]. Many physical properties, such as electrical conductivity, piezoelectricity, and defect structure, are greatly influenced by the composition of the material and the impurities and defects present in it.[20]

In this chapter; case of the Li-doped ZnO, there is a large difference in size between Zn and Li ions. It is expected that Li ions may occupy off-cantered positions, replacing the host Zn ions and forming electric dipoles. The structural modifications induced by Li dopant in ZnO greatly affect the electronic and dielectric properties. We realized that the study of frequency-dependent dielectric properties of Fe and Li co-doped ZnO materials is the least explored area till now and we, therefore, were motivated to take up this task. The major reason to choose Fe and Li co-doping is to

convert the material into a p-type semiconductor without creating stoichiometric oxygen defects in the lattice and make it robust against the oxidizing atmosphere. This paper reports the modification induced in structural, dielectric, and complex impedance properties of Fe and Li co-doped ZnO synthesized material by the sol-gel method.

5.2 Material Synthesis and Characterizations

In this chapter $Zn_{1-x}Fe_xO_{1+\delta}$ and $Zn_{1-2x}Li_xFe_xO$ ceramic samples were prepared by the conventional sol-gel method where; (x=0.05, 0.1). For the preparation of $Zn_{1-2x}Li_xFe_xO$, we have taken the stoichiometric amount of ZnO, Li_2CO_3, and $Fe(NO_3)_3$ in distilled water and mixed it with a magnetic stirrer at 70 °C. Then heated it to 100 °C on a hot plate and HNO_3 was to get ZnO dissolved resulting appearance of a transparent solution. Then we mixed melamine (1.2 times the total mole of cations present in the solution) for bonding/chelation between atoms. Then the solution was heated at 120 °C for 12 hours and gel-type material was obtained. Then it was kept in the oven at 200 °C for 8 hours to remove organic components. The solid material we got after that was ground in a mortar pestle and heated at 950 °C for 12 hrs. The heated powder was removed from the furnace after natural cooling till room temperature.

The phase formation study was carried out through a Rigaku Miniflex desktop X-ray diffractometer (XRD) with Cu-Kα radiation (λ = 1.54 Å) in the 2θ range of 30−70° with a step size of 0.02°. The microstructures of the sintered samples were investigated using scanning electron microscopy (SEM, EVO-scanning electron microscope MA15/18). The average grain size was calculated using the linear intercept method. The composition of the compounds was examined by energy

dispersive X-ray (EDX) spectroscopy with a probe attached to the SEM instrument. X-ray photoelectron spectroscopy (XPS) studies were carried out to examine the electronic structure of the materials. XPS of the samples were collected using a Thermo Scientific Multilab 2000 instrument by employing an Al-Kα radiation source operated at 150 kW. Binding energies were corrected and reported here with reference to C (1s) at 284.5 eV, and they are accurate within ±0.1 eV.

All samples were examined by using a Novocontrol Alpha-A frequency analyzer for dielectric measurements. The dielectric, modulus, and loss measurements as well as impedance measurements were carried out for all the samples. The measurements were done in the frequency range 1 Hz to 10^6 Hz in the temperature range of room temperature (25 ^oC) to 450 °C at regular intervals of 5 ^oC up to 220 °C and then regular intervals of 3°C. For the study, we did gold plating on the pellet and then put it in the Novo control Alpha-A frequency analyzer, and then we did heating by the furnace from room temperature to 450 $^\circ C$ and we took readings at the interval of 5 $^\circ C$ up to 220 $^\circ C$ and then we took reading at an interval of 3 $^\circ C$ till 450 $^\circ C$.

5.3 Structural Study

The structural parameters and phase purity have been studied using powder X-ray diffraction patterns. XRD patterns of $Zn_{1-x}Fe_xO_{1+\delta}$ and $Zn_{1-2x}Li_xFe_xO$is shown in Fig. 5.1(a) and (b). Sharp and intense diffraction peaks of all the samples confirm the high crystallinity of the samples. It also reveals a clean hexagonal phase formation (space group: P63mc) in wurtzite ZnO structure for full doping range in case $Zn_{1-2x}Li_xFe_xO$. Minute impurities phase of Fe_2O_3 were observed in powder XRD pattern in the case of Fe-doped ZnO samples.

Table 5.1. Structural Parameters of $Zn_{0.9}Fe_{0.1}O_{1+\delta}$ and $Zn_{0.8}Li_{0.1}Fe_{0.1}O$

Compound	Lattice Parameters (Å)		χ^2	R_f	R_{Bragg}	R_{wp}
	a=b	c				
$Zn_{0.9}Fe_{0.1}O_{1+\delta}$	3.2496(2)	5.2031(3)	2.34	6.84	7.21	15.4
$Zn_{0.8}Li_{0.1}Fe_{0.1}O$	3.2526(3)	5.2014(2)	1.80	6.32	6.56	11.7

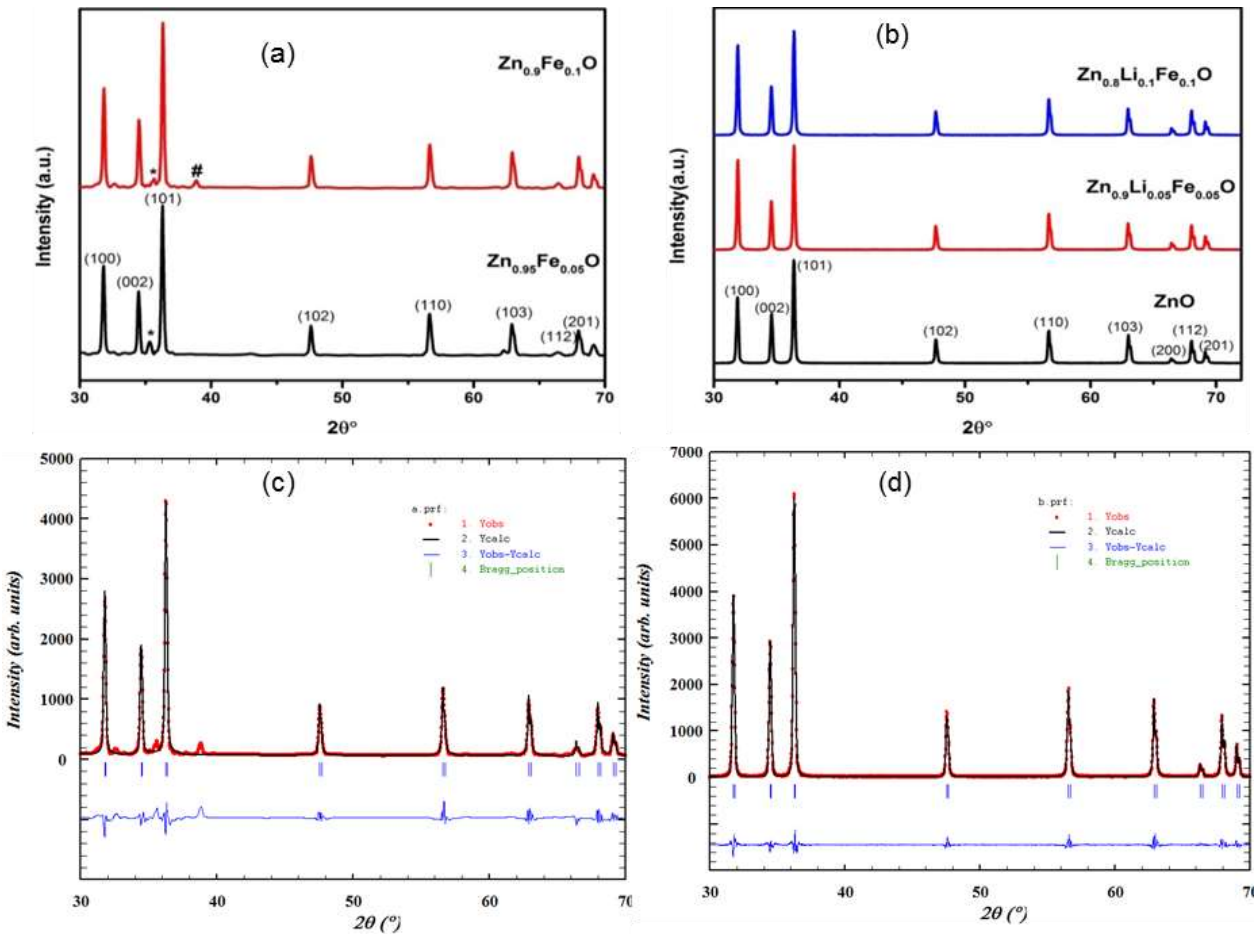

Fig. 5.1. Powder XRD sample of (a). $Zn_{1-x}Fe_xO_{1+\delta}$ and (b). $Zn_{1-2x}Li_xFe_xO$. Rietveld refined powder XRD pattern of (c). $Zn_{0.9}Fe_{0.1}O_{1+\delta}$ and (d). $Zn_{0.8}Li_{0.1}Fe_{0.1}O$

5.4 SEM and EDAX Study

The SEM study shown in Fig. 5.2(a) reveals that the grains are of sub-micrometer sizes in the range of 0.5-1μm for $Zn_{0.9}Fe_{0.1}O_{1+\delta}$ samples. The SEM study shown in Fig. 5.3(a) reveals the formation of grains of 2-50 μm sizes for the $Zn_{0.8}Li_{0.1}Fe_{0.1}O$ sample. The EDX image shown in Fig. 5.2(b) and 5.3(b) also

confirms the composition of the materials; however, Li peaks do not appear in the EDX image due to spectroscopic limitations in the EDX study.

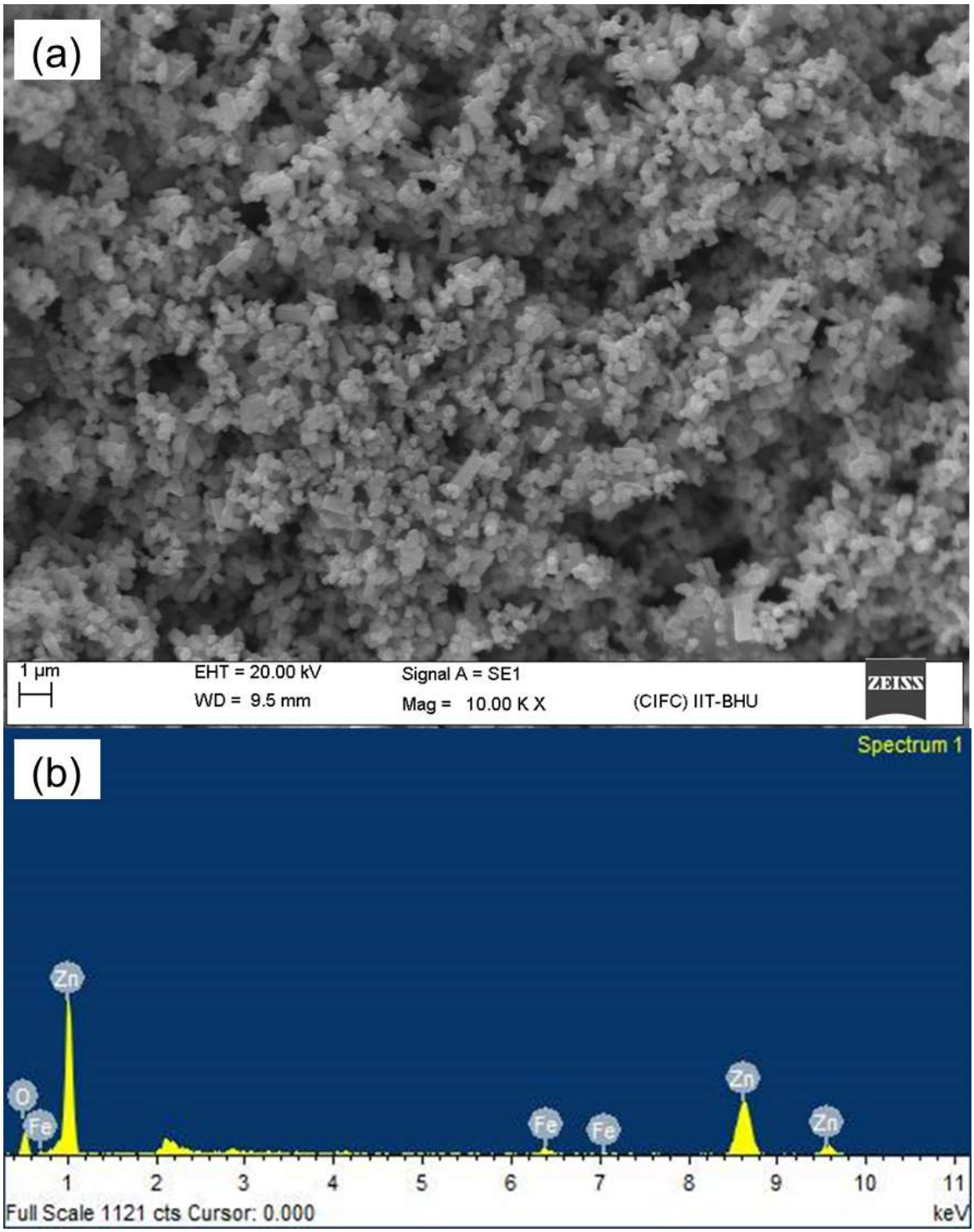

Fig. 5.2 (a). SEM image and (b). EDX image of $Zn_{0.9}Fe_{0.1}O_{1+\delta.}$

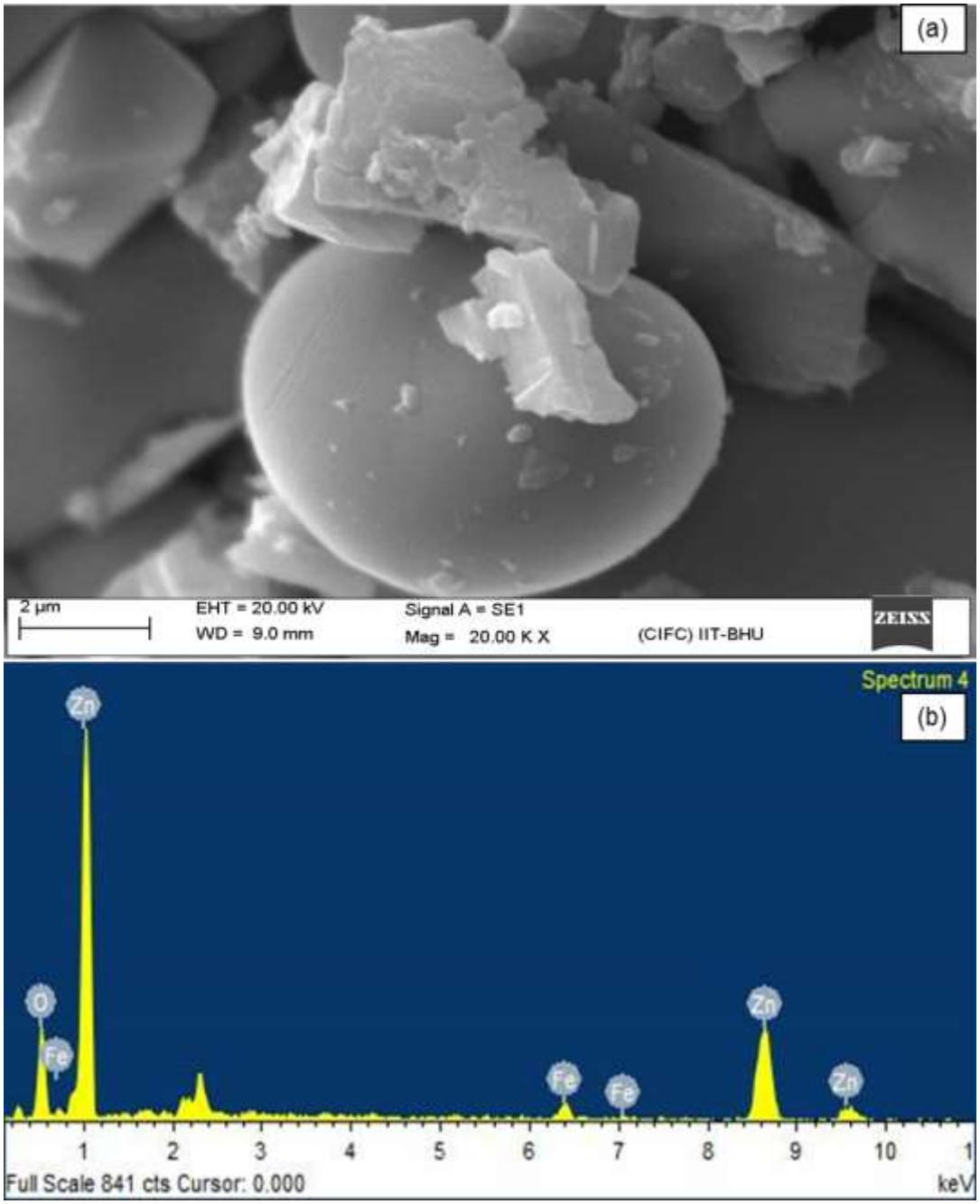

Fig. 5.3. (a). SEM image and (b). EDX image of $Zn_{0.8}Li_{0.1}Fe_{0.1}O$.

5.5 XPS Study

The electronic structure of $Zn_{0.8}Li_{0.1}Fe_{0.1}O$ was investigated by the XPS study. The deconvoluted Li(1s) and Fe(2p) spectra are shown in Figures 5.4 (a) and (c). Core level 1s peak lithium was observed at 55.4 eV confirming the presence of Li in the sample. The 2p3/2 peaks marked at 710.2 with the weak satellite at 717.1 eV and 2p1/2 at 723.8 eV with no satellite peak, respectively, confirm the presence of Fe^{3+} in

the sample. The 2p3/2 and 2p1/2 peaks at 1021.2 eV and 1044.8 eV respectively in Figure 5.4 (b) were assigned to Zn^{2+} ions. Figure 5.4(d) shows the O(1s) core level spectra. An estimation of the relative surface concentrations of Zn:Fe: Li was carried out from the intensities of Zn(2p), Fe(2p), and Li(1s) peaks in $Zn_{0.8}Fe_{0.1}Li_{0.1}O$.

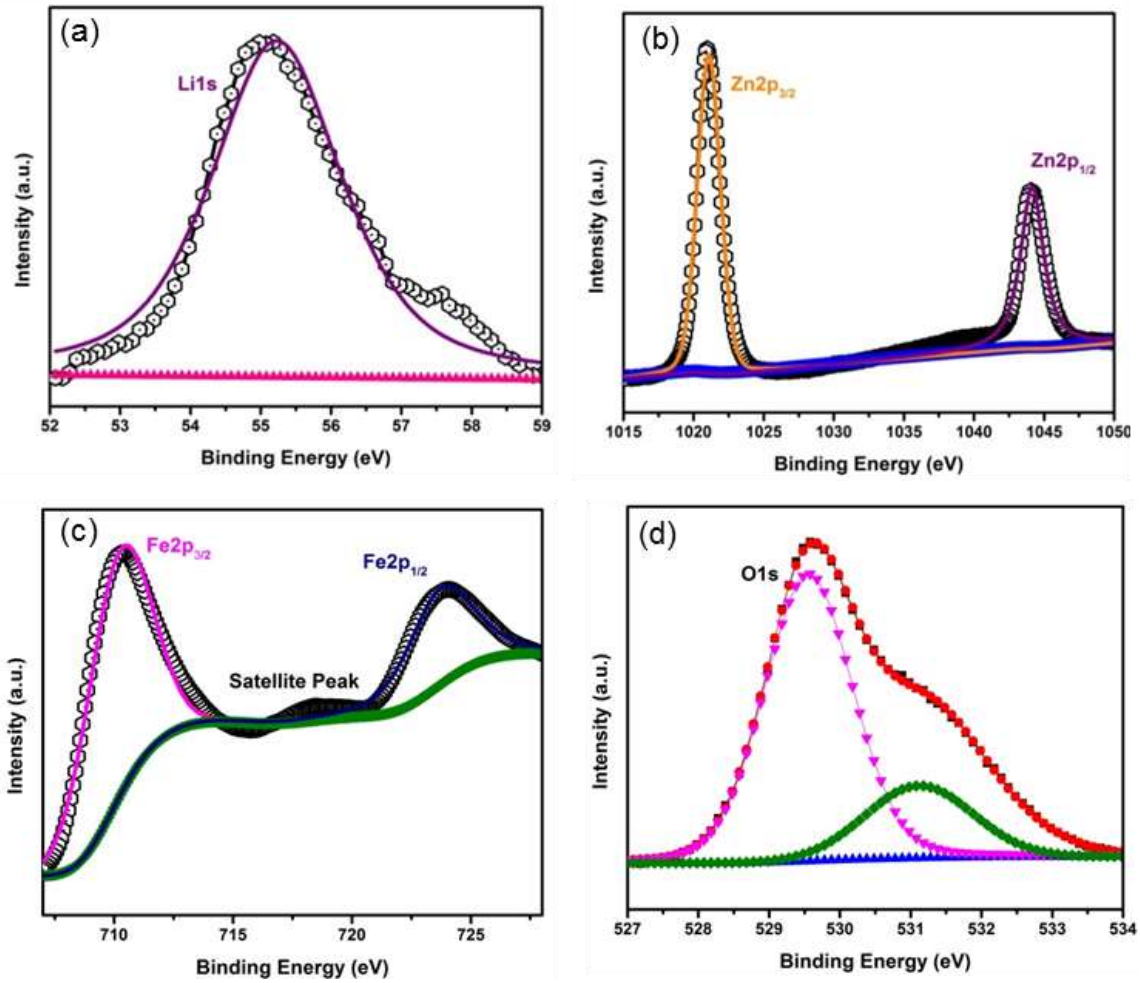

Fig: 5.4. XPS of $Zn_{0.8}Fe_{0.1}Li_{0.1}O$ (a) Core level of Li(1s), (b) Core level of Zn(2p), (c) Core level of Fe(2p), (d) Core level of O(1s).

5.6 Dielectric Study

The impedance spectroscopy was carried out at a variable temperature in the air to study the dielectric behavior of the material in the frequency range of 1 MHz to 1 kHz. The dielectric constant was calculated using the formula:

$$\varepsilon_r = \frac{C*d}{\varepsilon_\circ * A} \tag{5.1}$$

Where; ε_r is the dielectric constant, C is capacitance, ε_o is the permittivity of free space ($8.85*10^{-12}$)F/m, d is the thickness of the pellet, A is the area of the pellet;

Capacitance (C) was calculated by using the formula

$$C = -\frac{1}{\omega}\left[\frac{Z''}{Z'^2 + Z''^2}\right] \tag{5.2}$$

and the dielectric loss was calculated by

$$\tan\delta = \frac{\varepsilon''}{\varepsilon'} = \frac{Z'}{-Z''} \tag{5.3}$$

Figures 5.5(a) and 5.6(a) show the plots of the real part of the dielectric constant (ε_r') at the 1 kHz to 1 MHz frequency range for the $Zn_{0.9}Fe_{0.1}O_{1+\delta}$ and $Zn_{0.8}Li_{0.1}Fe_{0.1}O$ pellets in the temperature range of RT to 450 °C. In general, the ε_r' values were increasing in the range of RT to 400 °C with maxima appearing around 400 °C. The dielectric constant (ε_r') for $Zn_{0.9}Fe_{0.1}O_{1+\delta}$ is 612 and $Zn_{0.8}Li_{0.1}Fe_{0.1}O$ is 90000 respectively at 1000 Hz frequency at 400°C. The much lower dielectric constant of $Zn_{0.9}Fe_{0.1}O_{1+\delta}$ compared to $Zn_{0.8}Li_{0.1}Fe_{0.1}O$ may result in cation vacancies in oxygen excess lattice due to substitution Fe^{3+} on Zn^{2+} sites. That is why the codoping of Li^+ along with Fe^{3+} is important because Li^+ not only provides a charge balance that

diminishes the chances of the formation of stoichiometric vacancies/defects in the lattice but, due to the presence of multiple charge centers or different oxidation state elements in the same lattice, the differentiative net dipole moment is generated on different M-O bonds generating resultant dipole moment in the lattice or very high dielectric constant of the material. The variation in dielectric loss ($\tan \delta = \varepsilon_r''/\varepsilon_r'$) with temperature, at the selected frequency, is shown in Figures 5.5(b) and 5.6(b). Considering the high dielectric constant of the materials, the observed dielectric loss is quite less for $Zn_{0.9}Fe_{0.1}O_{1+\delta.}$ and $Zn_{0.8}Li_{0.1}Fe_{0.1}O$ samples. It was found that the dielectric constant was increasing continuously up to 400°C and dielectric loss was first increasing and then decreasing with temperature increment from 200°C to 400°C at all frequencies. However, both dielectric constant and dielectric loss were decreased with increasing frequencies. The increase in dielectric constant (ε_r') with increasing temperatures at different frequencies for $Zn_{0.9}Fe_{0.1}O_{1+\delta.}$and $Zn_{0.8}Li_{0.1}Fe_{0.1}O$ is likely due to the localized nature of hopping charge carriers in addition to interfacial polarization due to space charge. These extrinsic contributions to ε_r' are expected to contribute significantly only at higher frequencies. Further, it was also observed that from Fig. 5.7(a), (b), and 5.8(a), (b), plots of $Zn_{0.9}Fe_{0.1}O_{1+\delta}$ and $Zn_{0.8}Li_{0.1}Fe_{0.1}O$, at lower frequencies, high relative dielectric permittivity was found with obvious dispersion of dielectric properties. The large frequency dispersion never reached a low-frequency plateau. Inhomogeneities in grains and/or the presence of potential barriers between the grains are considered to be the reason for similar dielectric properties in several materials. Overall, doping of Fe^{3+} and Li^{+} in the ZnO lattice has proven to be an important strategy to improve the dielectric constant of the ZnO-based materials. Further co-doing Fe^{3+} and Li^{+} resulted in high k dielectric behavior in the materials.

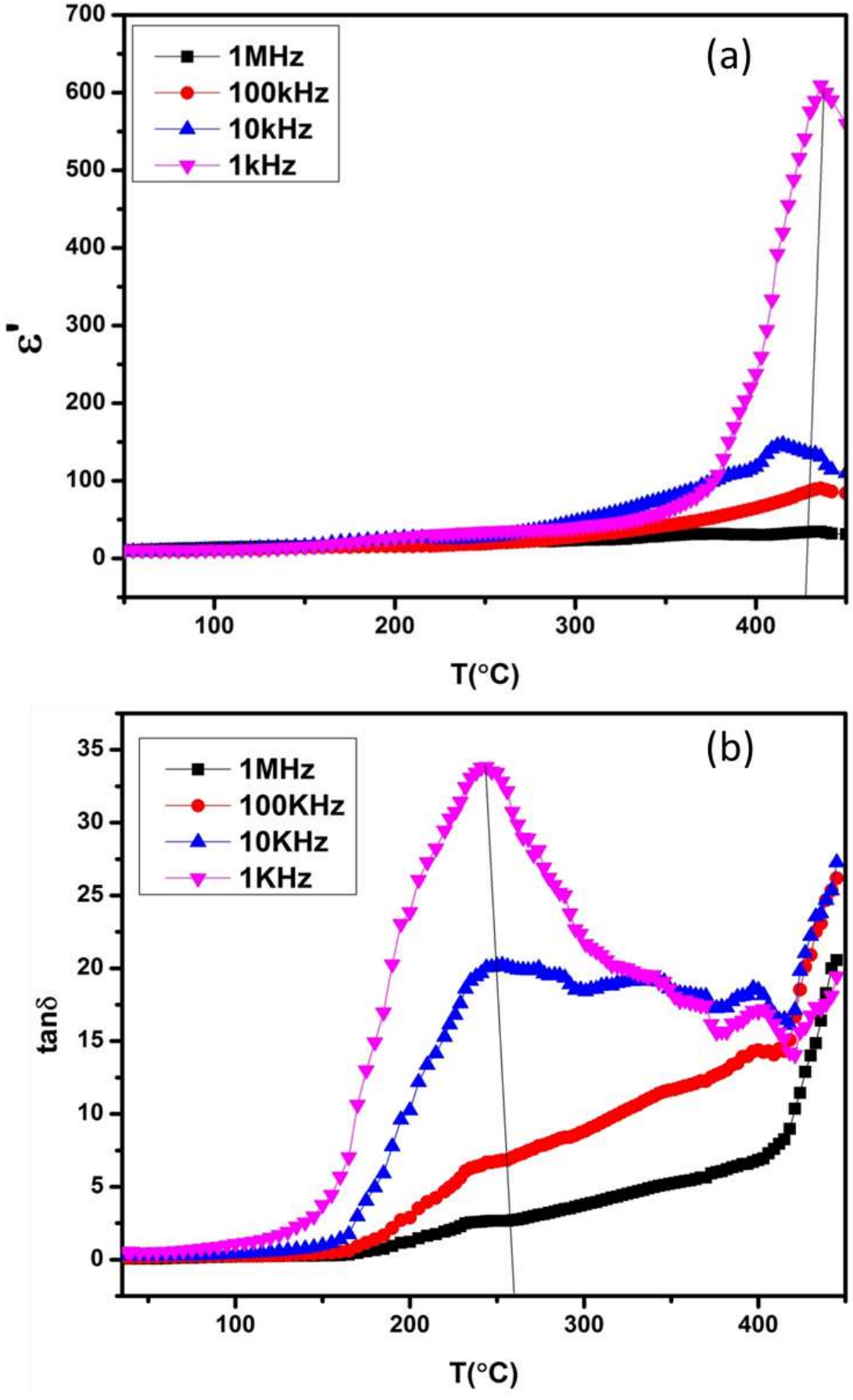

Fig. 5.5. (a). Dielectric constant and (b). Dilelectric loss of $Zn_{0.9}Fe_{0.1}O_{1+\delta}$.

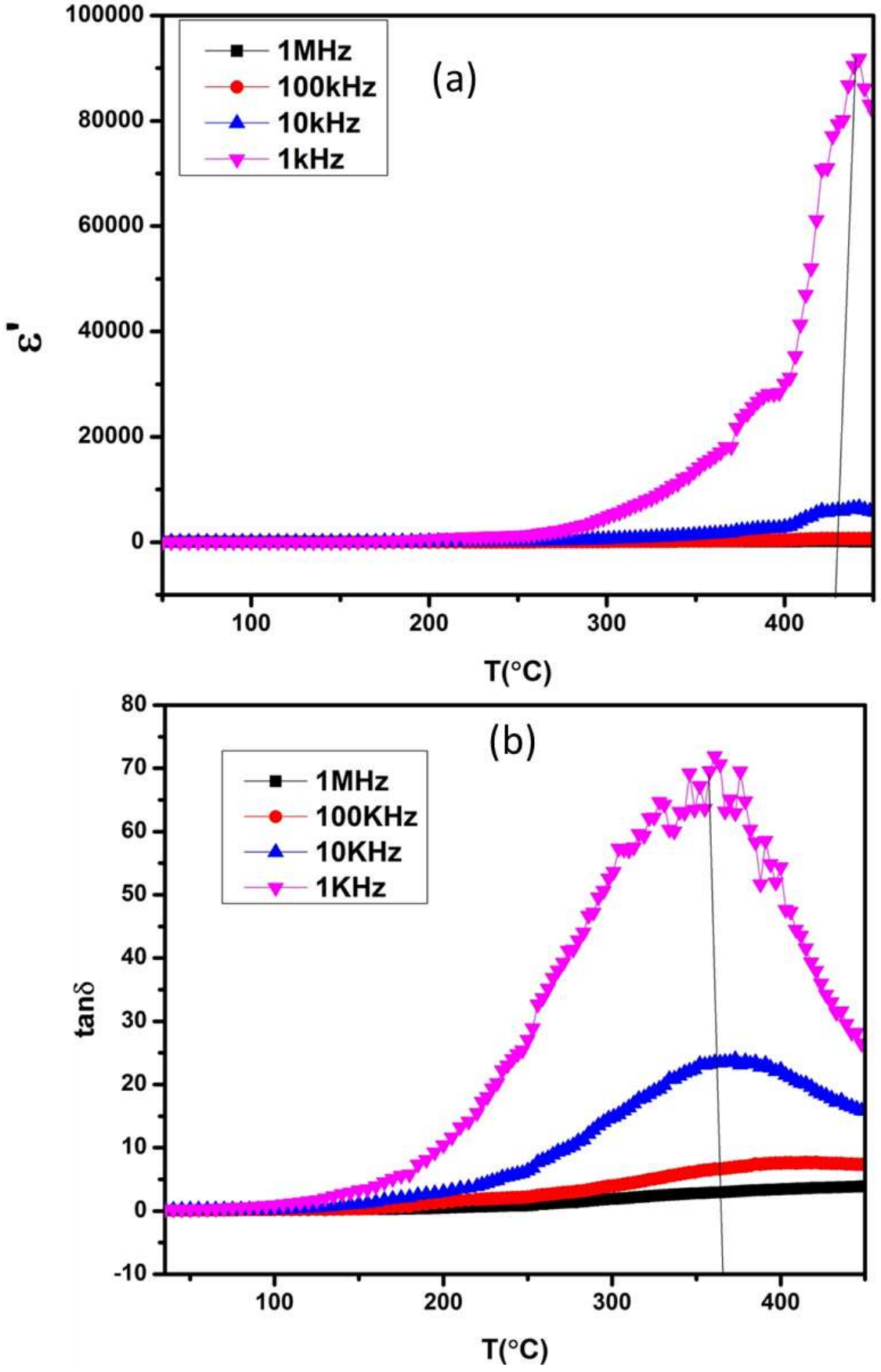

Fig. 5.6. (a). Dielectric constant and (b). Dilelectric loss of $Zn_{0.8}Li_{0.1}Fe_{0.1}O$.

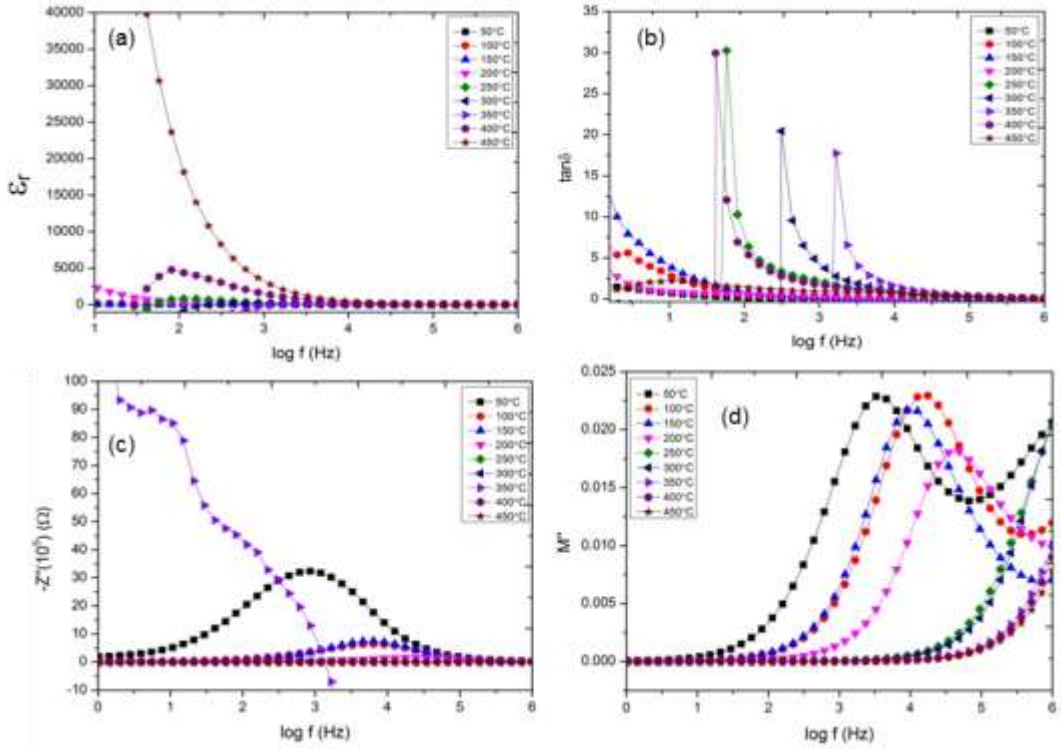

Fig. 5.7. (a). ε_r vs. log frequency plot, (b). tanδ vs. log frequency plot, (c). Z'' vs. log frequency plot and (d). M'' vs. log frequency plot of $Zn_{0.9}Fe_{0.1}O_{1+\delta}$

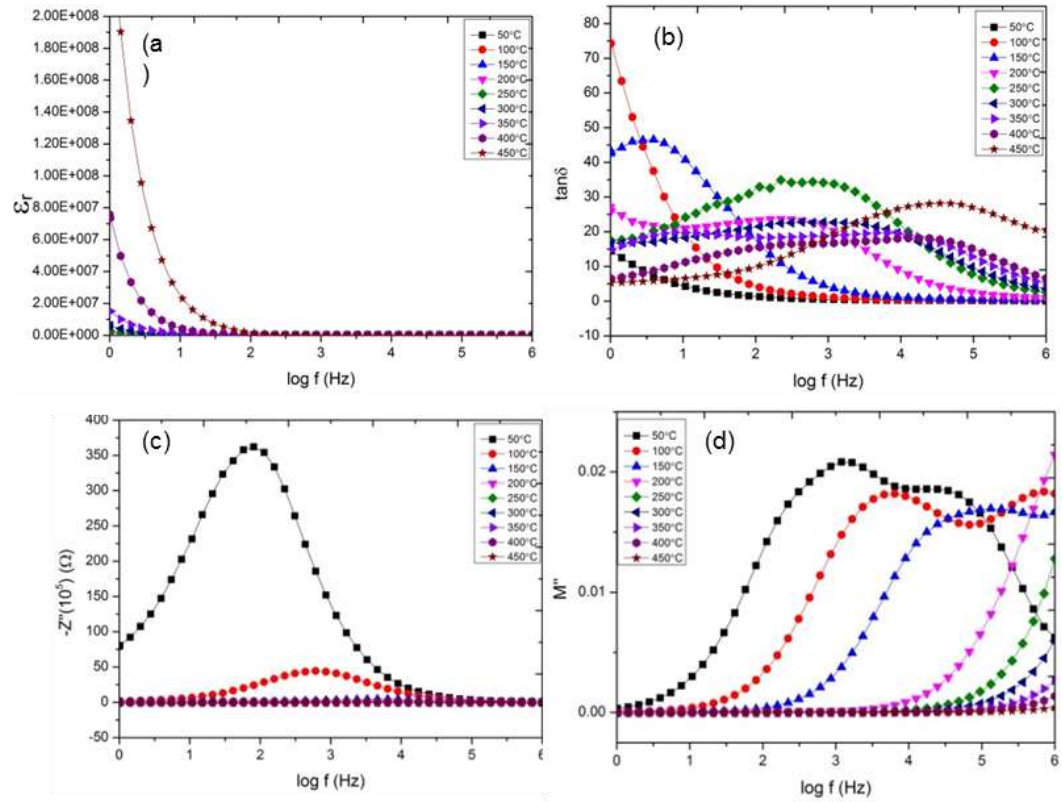

Fig. 5.8. (a). ε_r vs. log frequency plot, (b). tanδ vs. log frequency plot, (c). Z'' vs. log frequency plot and (d). M'' vs. log frequency plot of $Zn_{0.8}Li_{0.1}Fe_{0.1}O$.

5.7 Conclusion

In this chapter, we have successfully demonstrated the synthesis of single-phase Fe-doped ZnO and Fe/Li co-doped ZnO. In this work, $Zn_{1-x}Fe_xO_{1+\delta}$ and $Zn_{1-2x}Li_xFe_xO$ ceramics samples were prepared by the sol-gel method where x=0.10 and 0.05. However, we are not able to do more than 10% doping of Fe and Li in ZnO. The formation of single-phase wurtzite samples was confirmed by X-ray diffraction analysis. The microstructure of the material was analyzed by scanning electron microscopy which shows the polycrystalline nature of samples and the composition of the sample was analyzed by an EDX probe attached SEM instrument. The bulk, as well as the surface composition of the sample, was confirmed by the ICP-MS and XPS study. The electronic structure and oxidation state of the element present in the sample were confirmed by the XPS study. The complex impedance spectroscopic study of Fe-doped and Fe/Li co-doped ZnO shows a high dielectric constant and low dielectric loss at high temperatures and high frequency compared to ZnO. The Fe and Fe/Li doping depresses the concentration of the intrinsic donor and impedes the conduction mechanism resulting in The dielectric constant (ε_r') equivalent to 612 for $Zn_{0.9}Fe_{0.1}O_{1+\delta}$ and 90000 for $Zn_{0.8}Li_{0.1}Fe_{0.1}O$. at 1000 Hz frequency at 400^oC. Also with an increase in frequency, the dielectric constant and dielectric loss were found to decrease. This behavior was attributed to different hopping mechanisms and defects formed during synthesis.

REFERENCES

[1] R. S. Ganesh, E. Durgadevi, M. Navaneethan, et al., "Low-temperature ammonia gas sensor based on Mn-doped ZnO nanoparticle decorated microspheres," Journal of Alloys and Compounds, vol. 721, (2017) pp. 182–190.

[2] N. Sekine, C. H. Chou, W. L. Kwan, and Y. Yang, "ZnO nano-ridge structure and its application in inverted polymer solar cell," Organic Electronics, vol. 10, no. 8, (2009) .pp.1473–1477.

[3] H. Kim, A. Pique, J. S. Horwitz, et al., "Effect of aluminum doping on zinc oxide thin films grown by pulsed laser deposition for organic light-emitting devices," Thin Solid Films, vol. 377-378, (2000). pp. 798–802.

[4] M. Suchea, S. Christoulakis, K. Moschovis, N. Katsarakis, and G. Kiriakidis, "ZnO transparent thin films for gas sensor applications," Thin Solid Films, vol. 515, no. 2, (2006). pp. 551–554.

[5] P. Chesler, C. Hornoiu, S. Mihaiu et al., "Nanostructured SnO2–ZnO composite gas sensors for selective detection of carbon monoxide," Beilstein Journal of Nanotechnology, vol. 7, (2016), pp. 2045–2056.

[6] Z. L. Wang and J. Song, "Piezoelectric nanogenerators based on zinc oxide nanowire arrays," Science, vol. 312, no. 5771, (2006), pp. 242–246.

[7] M. A. Awad, E. M. M. Ibrahim, and A. M. Ahmed, "One step syntheses of S incorporated ZnO nanowires for photocatalysis applications," European Physical Journal Applied Physics, vol. 72, no. 3, (2015), article 30303.

[8] N. Kumar, A. Dorfman, and J. Hahm, "Ultrasensitive DNA sequence detection using nanoscale ZnO sensor arrays," Nanotechnology, vol. 17, no. 12, (2006), pp. 2875–288.

[9] M. S. Arnold, P. Avouris, Z. W. Pan, and Z. L. Wang, "Field-effect transistors based on single semiconducting oxide nanobelts," The Journal of Physical Chemistry B, vol. 107, no. 3, (2003), pp. 659–663.

[10] C.C. Homes, T. Vogt, S.M. Shapiro, S. Wakimoto, A.P. Ramirez Optical response of high-dielectric-constant perovskite-related oxide Science, 293 (2001), pp. 673-676

[11] R. Tripathi, A. Kumar, C. Bharti, T.P. Sinha Dielectric relaxation of ZnO nanostructure synthesized by soft chemical method Curr. Appl. Phys., 10 (2010), pp. 676-681

[12] M.K. Gupta, B. Kumar Enhanced ferroelectric, dielectric and optical behavior in Li-doped ZnO nanorods J. Alloys Compd., 509 (2011), pp. L208-L212

[13] G. Corro, S. Cebada, F. Bañuelos, J.L.G. Fierro, U. Pal, E. Guilleminot, Low-cost Cu/ZnO as low temperature (150 °C) catalyst for diesel particulate matter oxidation. Top. Catal. 59(2016), 1090–1094.

[14] S.M. Mohammad, Z. Hassan, N.M. Ahmed, N.H. Al-Hardan, M. Bououdina, Fabrication of low-cost UV photodetector using ZnO nanorods grown onto nylon substrate. J. Mater. Sci. Mater. Electron 26(2015), 1322–1331.

[15] K.H. Choi, M. Mustafa, K. Rahman, B.K. Jeong, Y.H. Doh, Cost-effective fabrication of memristive devices with ZnO thin film using printed electronics technologies. Appl. Phys. A 106(2012), 165–170.

[16] J.V. Gohel, A.K. Jana, M. Singh, Highly enhanced photocurrent of novel quantum-dot-co-sensitized PbS–Hg/CdS/Cu: ZnO thin films for photoelectrochemical applications. Appl. Phys. A 123 (2017), 506.

[17] C. Karunakaran, A. Vijayabalan, P. Vinayagamoorthy, CdOimplanted hexagonal ZnO nanoplatelets: red-shifted emission and enhanced charge carrier-resistance and bacteria-inactivation. Appl. Phys. A 14 (2018), 125.

[18] R. Uma, K. Ravichandran, S. Sriram, B. Sakthivel, Cost-effective fabrication of ZnO/g-C_3N_4 composite thin films for enhanced photocatalytic activity against three different dyes (MB, MG, and RhB). Mater. Chem. Phys. 201(2017), 147–155.

[19] S. Snega, K. Ravichandran, N.J. Begum, K. Thirumurugan, Enhancement in the electrical and antibacterial properties of sprayed ZnO films by simultaneous doping of Mg and F. J. Mater. Sci. Mater. Electron. 24(2013), 135–141.

[20] X.S. Wang, Z.C. Wu, J.F. Webb, Z.G. Liu, Ferroelectric and dielectric properties of Li-doped ZnO thin films prepared by pulsed laser deposition, Appl. Phys. A: Mater. Sci. Process., 77 (2003), pp. 561-565